

Hollow Mesoporous Silica Nanocarriers with Multifunctional Capping Agents for In Vivo Cancer Imaging and Therapy

Shun Yang, Dongyun Chen,* Najun Li, Qingfeng Xu, Hua Li, Frank Gu, Jianping Xie,* and Jianmei Lu*

Efficient drug loading and selectivity in drug delivery are two key features of a good drug-carrier design. Here we report on such a drug carrier formed by using hollow mesoporous silica nanoparticles (HMS NPs) as the core and specifically designed multifunctional amphiphilic agents as the encapsulating shell. These nanocarriers combine the advantages of the HMS NP core (favorable physical and structural properties) and the versatility of an organic-based shell (e.g., specificity in chemical properties and modifiability). Moreover, both the properties of the core and the shell can be independently varied. The varied core and shell could then be integrated into a single device (drug carrier) to provide efficient and specific drug delivery. In vitro and in vivo data suggests that these drug nanocarriers are biocompatible and are able to deliver hydrophobic drugs selectively to target tumor cells. After the break of the pH-labile linkages in the shell, the drug payload can be released and the tumor cells are killed.

Dr. S. Yang, Prof. D. Chen, Prof. N. Li, Prof. Q. Xu,
Prof. H. Li, Prof. J. Lu
College of Chemistry
Chemical Engineering and Materials Science
Collaborative Innovation Center of Suzhou Nano
Science and Technology
Soochow University
Suzhou 215123, P. R. China
E-mail: dychen@suda.edu.cn; lujm@suda.edu.cn

Prof. J. Xie
Department of Chemical & Biomolecular Engineering
Faculty of Engineering
National University of Singapore
117576, Singapore
E-mail: chexiej@nus.edu.sg

Prof. F. Gu
Department of Chemical Engineering
Waterloo Institute for Nanotechnology
University of Waterloo
Ontario N2L 3G1, Canada
DOI: 10.1002/smll.201503121



1. Introduction

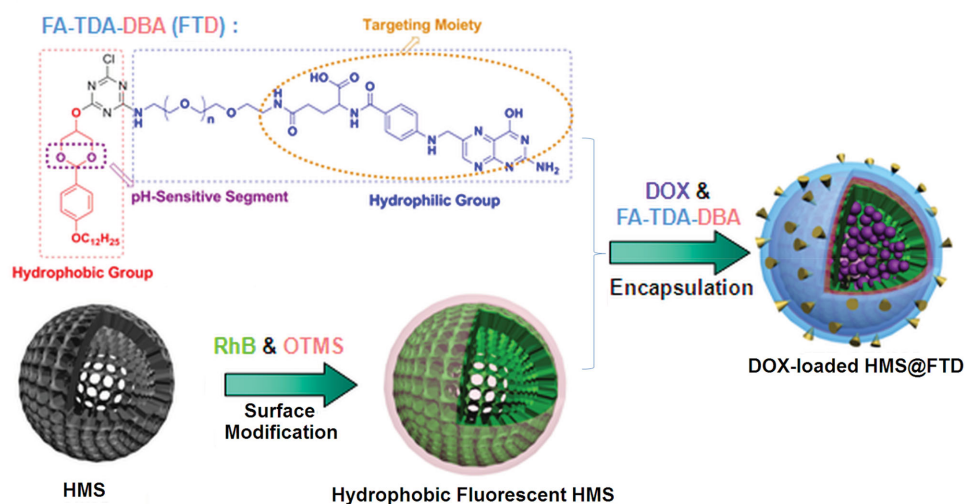
Current interest in the development of drug-delivery systems has shifted toward multifunctional drug carriers, as hybrid drug carriers with diagnostic and therapeutic modalities (or theranostic carriers) have shown significant improvement in diagnostic accuracy and antitumor efficacy.^[1–4] Drug carriers of nanometer size (or nanocarriers) are ideal for this purpose as they provide a particularly efficient platform to integrate multiple functionalities, including targeting, imaging, and therapy (or more), into a single entity. Efficient drug loading and selective drug delivery are two key features for a good design of drug nanocarriers. Here we report a unique core-shell nanocarrier structure, where the complementary features of the two key components – inorganic nanoparticles (NPs, as the core) and functional organic moieties (as the capping shell) can be independently designed and integrated into a single nanocarrier to achieve efficient and specific cancer therapy. By using inorganic nanoparticles,

the nanocarriers could achieve a high drug loading content. Moreover, the functional organic moieties could be designed to be biodegradable/biocompatible, to specifically target disease sites, and to be sensitive to the environmental conditions. These core-shell nanocarriers could thus be employed for efficient drug uptake, targeted drug delivery, and effective cancer therapy, with improved performance in cancer management compared with conventional therapeutics.^[5,6]

Hollow mesoporous silica (hereafter referred to as HMS) NPs were chosen in this study as the drug carrier. Inorganic NPs, such as gold, magnetic, and silica nanoparticles, have been widely used as drug carriers owing to their facile synthesis, good colloidal stability, and excellent structural rigidity.^[7–11] In particular, mesoporous silica NPs, which also feature a high porosity (or large surface area), tunable pore morphology (size and structure), and facile surface modification, have recently emerged as an ideal nanocarrier for drug delivery.^[12] By using a hollow structure for the mesoporous silica NPs (termed hollow mesoporous silica or HMS NPs), the drug-loading capacity and drug-releasing profile could be further improved, where the free volume in the hollow inner of the HMS NPs can improve the drug loading capacity and the mesoporous layer of the NPs can provide a sufficient and controlled diffusion path for the drug payloads. Furthermore, the size and shape of the hollow inner, and the thickness (or diffusion length) and pore morphologies of the mesoporous layer, can be independently fine-tuned to achieve an optimal drug loading and releasing profile in a particular bio-setting. One key challenge in the use of HMS NPs as drug carriers is the potential toxicity of unmodified silica NPs. This challenge has been recently addressed by incorporating a polymer coating on the silica NP surface.^[13–17] However, using a thick polymer-coating layer on the HMS NP surface may constrain the drug loading and releasing from the HMS nanocarriers. Therefore, there is a strong interest in the design of “smart” and efficient capping layers for the HMS nanocarriers to achieve a selective and controlled drug release.^[18,19]

The incorporation of stimuli-responsive moieties in the capping layers is most attractive in this perspective.^[20–25] Biodegradable capping layers, which degrade in response to a particular external stimulus, such as temperature, pH, and enzymatic or photochemical reactions, have recently been used in nanocarrier design to achieve a controlled release of drug payloads within the affected cells.^[26,27] For example, pH-responsive moieties were used for a controlled release of drug payloads in a slightly acidic environment (pH 5.0–6.5) of endosomes or lysosomes inside affected cells.^[28–30] A variety of amphiphilic polymers with pH-labile linkages have been recently developed to achieve the controlled release of drug payloads within cells. The selective delivery of drug carriers to cancer cells can be further realized by incorporating a cancer-targeting ligand, such as folic acid, arginylglycylaspartic acid (RGD) peptides, sugars or antibodies, to the amphiphilic polymers.^[31–37]

Herein, we report a novel core-shell structured nanocarrier consisting of a hydrophobic fluorescent HMS NP as the core and well-designed, multifunctional amphiphilic agents as the capping shell for selective and controlled drug delivery. Two key elements that can be independently designed and tailored have thus been incorporated in our nanocarrier design. As shown in **Scheme 1**, the first element is a hydrophobic fluorescent HMS NP, which provides an excellent drug-loading capacity and drug-releasing profile. The second element is an amphiphilic capping agent consisting of four functional motifs: a targeting segment (folic acid, FA), a hydrophilic segment (4,7,10-trioxo-1,13-tridecanediamine, TDA), a pH-labile linkage, and a hydrophobic segment (4-n-dodecyloxybenzalacetal, DBA), as illustrated in Scheme 1. The as-designed multifunctional amphiphilic capping agents are hereafter referred to as **FA-TDA-DBA** or **FTD** for short. HMS is easily encapsulated by FTD to form **HMS@FTD** because of the strong interaction between the hydrophobic HMS NP and the hydrophobic segment of the FTD, and doxorubicin (DOX) can also be loaded to form **DOX-loaded HMS@FTD** in this process. The FTD capping



Scheme 1. Schematic illustration of the two key components in the design of the HMS@FTD drug nanocarriers: hydrophobic fluorescent HMS NPs and multifunctional amphiphilic FTD capping ligands.

agents can provide good protection for the HMS nanocarriers in bio-fluids. They also make the specific targeting of cancer cells (because of the FA moieties) possible, as well as the subsequent controlled release of drug payloads (from the pH-responsive moieties) in the affected cells.

2. Results and Discussion

The fabrication of monodisperse HMS NPs (ca. 150 nm diameter) was carried out according to our previous procedure, where polystyrene NPs (125 nm), tetraethyl orthosilicate (TEOS), and cetyltrimethylammonium bromide (CTAB) were used as the hollow-generating NPs, silica precursors, and pore-generating agents, respectively.^[12] The pristine HMS NPs were further incorporated with a fluorescent dye (e.g., red-emitting rhodamine B, RhB) to form fluorescent HMS NPs. A long-chain hydrophobic ligand octadecyltrimethoxysilane (OTMS) was then crafted on the surface of the fluorescent HMS NPs, which led to a remarkable wettability change of the NP surface—from highly hydrophilic to hydrophobic. Such surface modification could improve the hydrophobic interactions between the HMS NPs and the amphiphilic FTD capping agents (via their hydrophobic segments). The hydrophobic nature of the NP surface can also increase the adsorption of the hydrophobic drugs, which could lead to a better control of the drug release.

The detailed synthesis and characterization of the amphiphilic FTD capping agents are presented in the Experimental

Section (Figure S1 in the Supporting Information). The as-designed amphiphilic capping agents provide a good protection for the loaded drugs inside the HMS nanocarriers, which could largely inhibit the premature release of the drug. The core-shell drug nanocarriers were formed via self-assembly of the hydrophobic fluorescent HMS NPs, hydrophobic drugs (DOX), and amphiphilic FTD capping agents, based upon the strong hydrophobic interactions between DOX and the alkyl chains on the HMS NP surface (C18) and in the FTD capping agents (C12).^[38–40] The hydrophobic drugs were encapsulated inside the HMS NPs, and their release could be blocked by the FTD capping agents on the NP surface. It should be mentioned that the as-fabricated drug nanocarriers with a high content of FA ligands showed a poor solubility in aqueous solution because of the hydrogen bonding and π - π stacking between the FA ligands. To address this issue, an FA-free amphiphilic ligand, TDA-DBA (or TD), was used as a co-capping agent to the FTD ligands to improve the water solubility of the as-fabricated drug nanocarriers. The ideal mole ratio of FTD to TD ligands was determined to be 5:95. This optimized ratio was used in our further study. The as-fabricated drug nanocarriers are hereafter referred to as DOX-loaded HMS@FTD nanocarriers. The as-fabricated drug carriers showed excellent solubility and stability in aqueous solutions (pH 7) and in various buffer solutions (e.g., phosphate buffer).

Transmission electron microscopy (TEM) was used to examine the morphology and structure of the pristine HMS NPs, hydrophobic fluorescent HMS NPs, and DOX-loaded HMS@FTD nanocarriers. As shown in **Figure 1a**, nearly

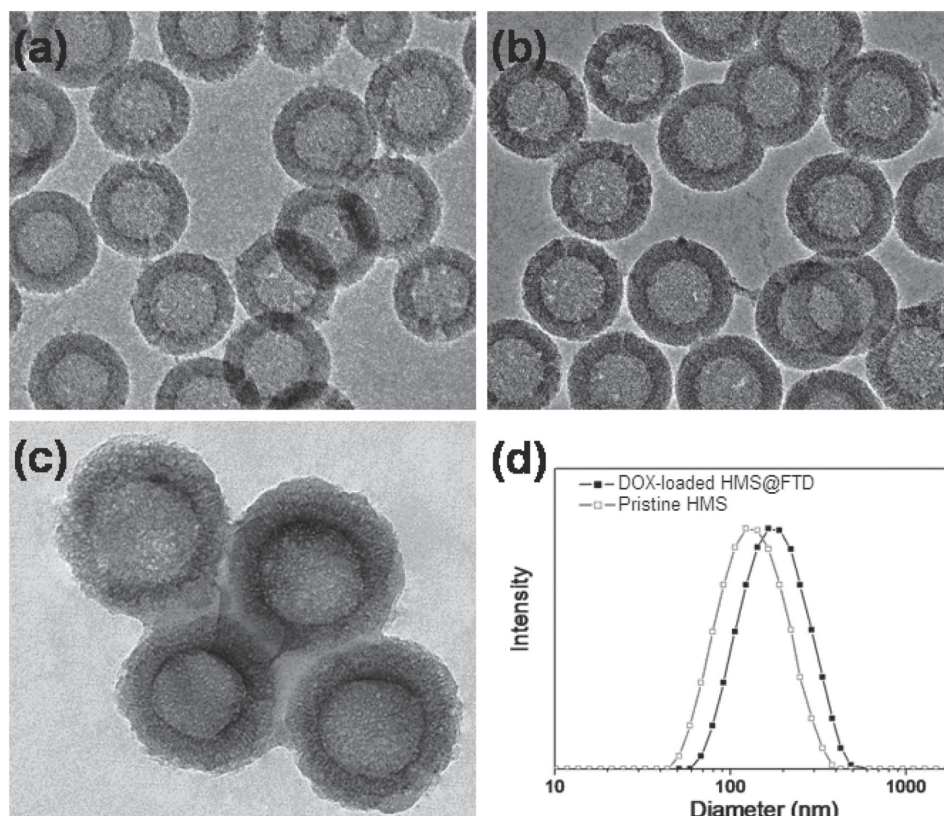


Figure 1. a–c) Representative TEM images of pristine HMS NPs (a), hydrophobic fluorescent HMS NPs (b), and DOX-loaded HMS@FTD nanocarriers (c); d) Dynamic light scattering analysis of the pristine HMS NPs and DOX-loaded HMS@FTD nanocarriers.

monodisperse spherical particles with a diameter of around 150 nm were observed for the pristine HMS NPs.^[41,42] A strong contrast between the edge (darker, ca. 20 nm in thickness) and the center (lighter, ca. 110 nm in diameter) could also clearly be observed in the NPs, implying the hollow structure of the pristine HMS NPs. The incorporation with the fluorescent dyes and the modification with the hydrophobic ligands had negligible effects on the morphology and structure of the HMS NPs, as evidenced by TEM (Figure 1b). However, the particle size of the HMS@FTD nanocarriers increased from around 150 nm (the pristine HMS NPs) to around 155 nm, as shown in Figure 1c. The increase in particle size was also supported by dynamic light scattering (DLS, Figure 1d) analyses of the pristine HMS NPs and HMS@FTD nanocarriers. In addition, compared to the pristine HMS NPs (Figure 1a), where the pore structure can be clearly identified, the pore structure in the HMS@FTD nanocarriers (Figure 1c) was very difficult to detect. This change in pore structure suggests the successful capping of the FTD ligands on the HMS NPs. The blocking of the pores by the FTD capping ligands could therefore provide a better protection for the loaded drugs inside the HMS nanocarriers. The successful capping of the FTD ligands on the HMS NPs was also substantiated by thermogravimetric analysis (TGA) of the HMS@FTD nanocarriers, where the capping ligands contributed about 13% of the weight of the nanocarriers. In contrast, the organic moieties contributed to only 4% of the weight of the nanocarriers in the pristine HMS NPs.

Fourier-transform infrared spectroscopy (FTIR) provided yet another line of evidence for the successful capping of the FTD ligands and loading of the hydrophobic drugs (DOX) in the HMS@FTD nanocarriers. As shown in Figure S2 (Supporting Information), a distinct peak at around 1750 cm^{-1} was observed in the FTIR spectrum of DOX-loaded HMS@FTD nanocarriers (bottom line). This peak could be assigned to the vibration stretching of the amide group in folic acid, which implied the successful capping of the FTD ligands on the HMS NPs. In addition, three absorption peaks at 1405, 1612, and 1070 cm^{-1} , which corresponded well to the carbonyl groups in quinine and ketone of DOX,^[43] were enhanced significantly in the FTIR spectrum of DOX-loaded HMS@FTD nanocarriers compared to that of OTMS modified fluorescent HMS (OFHMS). This data confirmed the successful loading of DOX in the HMS@FTD nanocarriers.

Confocal laser scanning microscopy (CLSM) was further used to confirm the successful encapsulation of DOX inside the HMS@FTD nanocarriers. The as-prepared DOX-loaded HMS@FTD was used without any further treatment after centrifugation in this study. DOX shows red fluorescence with a respective excitation and emission wavelength of 485 and 592 nm. To differentiate the fluorescence of the loaded DOX (red emission) from that of the fluorescent HMS nanocarriers, the nanocarriers were labeled with a green-emitting organic dye, fluorescein isothiocyanate (FITC). Both green (Figure 2a, $\lambda_{\text{em}} = 518$ nm) and red (Figure 2b, $\lambda_{\text{em}} = 592$ nm) fluorescence was observed in the DOX-loaded HMS@FTD nanocarriers under an excitation wavelength of 485 nm. This data provides more supportive evidence for the successful loading of DOX in the HMS@FTD nanocarriers.

The loading efficiency and capacity of DOX in the HMS@FTD nanocarriers were determined by UV-vis spectroscopy to be 89.4% and 158.9 μg DOX per mg of nanocarriers, respectively. The drug-loading efficiency was much higher when compared to traditional drug-delivery systems (e.g., mesoporous silica nanoparticles and micelles).^[44] The loaded DOX in the HMS@FTD nanocarriers was very stable in PBS buffer at physiological pH (7.4). As shown in Figure 3, the release of the loaded DOX was negligible at pH 7.4 even after a long (100 h) incubation time. This result also confirms that DOX was loaded into the nanoparticles instead of on the surface of the nanoparticles. Moreover, at pH 5.0 (Figure 3), a fast release of DOX was triggered in the HMS@FTD nanocarriers over the first 10 h, implying a fast hydrolysis of the amphiphilic capping ligands (FTD) at the slightly acidic pH. The TEM images of the degraded HMS@FTD nanoparticles at pH 5.0 are shown in Figure S3 (Supporting Information). It can be seen that the FTD capping ligands have detached from the HMS, and the pores have become uncovered, which further confirms that the release of DOX was caused by the pH-induced removal of folic acid from the particles. The strongly pH-dependent release profile of the HMS@FTD nanocarriers provides an ideal platform for selective and controlled drug delivery, where the drug release can be largely inhibited during circulation in the blood at physiological pH, and the loaded drugs will only be unloaded when the nanocarriers reach the targeted cells and will then be transported into the cells. In addition, a more sustained drug release profile was observed in the HMS@FTD nanocarriers compared to that of pristine HMS nanocarriers, further suggesting the

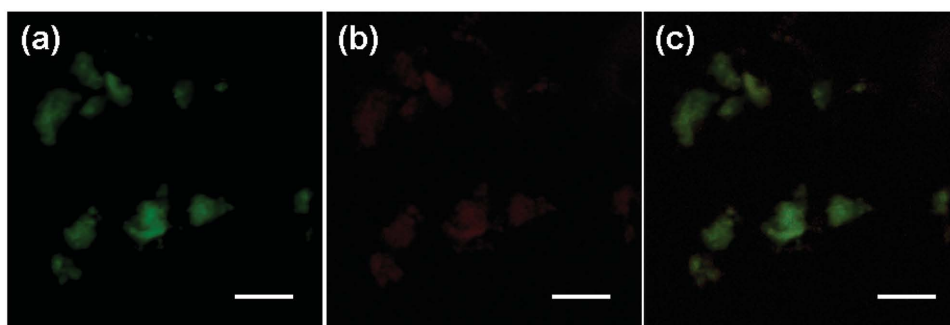


Figure 2. CLSM images of DOX-loaded HMS@FTD nanocarriers under different emission wavelengths ($\lambda_{\text{ex}} = 485$ nm): a) $\lambda_{\text{em}} = 518$ nm for green-emitting FITC; b) $\lambda_{\text{em}} = 592$ nm for red-emitting DOX; and c) physically overlaid image of the panels (a) and (b). Scale bar: 5 μm .

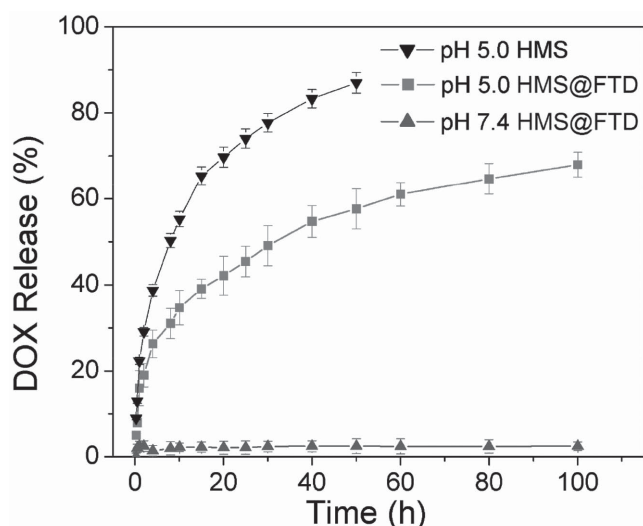


Figure 3. DOX release profiles of DOX-loaded pristine HMS NPs and HMS@FTD nanocarriers at pH 5.0 and 7.4.

crucial role of the hydrophobic surface modification and the as-designed FTD capping ligands on the NP surface. Even though the HMS@FTD did not fully release the loaded DOX within 100 h as opposed to the pristine HMS nanocarriers, the therapeutic efficacy of the HMS@FTD nanocarriers would be much higher than that of the pristine HMS nanocarriers due to the pH-controlled release. The as-designed HMS@FTD nanocarriers provide an excellent platform for well-controlled drug release, which could further be used to achieve good long-term antitumor efficacy.

The HMS@FTD nanocarriers also showed good biocompatibility. KB cells were chosen as the model cancer cell line to evaluate the potential cytotoxicity of the drug carriers. The KB cells were first treated with DOX-free HMS@FTD nanocarriers in different concentrations for 24 h, and the viability of the cells was measured using a sulforhodamine B (SRB) assay. As shown in Figure 4a, a very low cytotoxicity (cell viability >90% after 24 h incubation) was observed for DOX-free HMS@FTD nanocarriers even at a high dosage concentration (500 $\mu\text{g mL}^{-1}$). This good biocompatibility of the HMS@FTD nanocarriers can be ascribed to the non-toxic feature of the as-designed amphiphilic FTD capping agents.

To further evaluate the targeting capability of the HMS@FTD nanocarriers, KB cells with over-expressed folate receptors were treated with DOX-loaded HMS@FTD nanocarriers, DOX-loaded HMS@TD nanocarriers (without the FA moieties in the capping agents), and free DOX in different concentrations (5, 10, and 20 $\mu\text{g DOX mL}^{-1}$) for 24 h. As shown in Figure 4b, the viability of the KB cells depended strongly on the DOX dosage. The DOX-loaded HMS@FTD nanocarriers (Figure 4b, middle columns) showed nearly the same cytotoxicity against the KB cells as free DOX (right-hand columns) at different levels of DOX dosage. This value was much higher than that of the DOX-loaded HMS@TD nanocarriers without the FA ligands (left-hand columns). The obvious difference in cytotoxicity between the HMS@FTD nanocarriers and HMS@TD nanocarriers suggests the high selectivity of the FA ligands toward the KB cells. The HMS@FTD nanocarriers (with the FA ligands) were able to specifically target the KB cells with over-expressed folate receptors, and they can be uptaken by the cells via a direct folate-receptor-mediated endocytosis pathway.^[45–47] This active transport pathway is more efficient than the non-specific and passive endocytosis pathway, leading to an improved cytotoxicity to the KB cells.

The targeting efficacy of the FA ligands was further confirmed by CLSM and flow cytometry studies. Human hepatoma 7402 cells without over-expressed folate receptors were chosen as a negative cell line. The red fluorescence of DOX was used to monitor the intracellular activity of the drug nanocarriers. The KB cells and 7402 cells were treated with DOX-loaded HMS@FTD nanocarriers (FA-conjugated) and HMS@TD nanocarriers (FA-free) at the same DOX concentration of 10 $\mu\text{g mL}^{-1}$. The red fluorescence of the nanocarriers inside the cells was monitored by CLSM over a period of 3 h. As shown in Figure 5a and 5b (top panel), no obvious difference in the fluorescence intensity was detected for the DOX-loaded HMS@FTD nanocarriers in the KB and 7402 cells at 0.5 h. The possible reason is that, at the early stage of incubation (ca. 0.5 h), the KB and 7402 cells might uptake the drug nanocarriers via a similar non-specific and passive endocytosis pathway. Similarly, some red fluorescence intensity was also observed for the DOX-loaded HMS@TD nanocarriers in the KB cells (Figure 5c, top panel). However, after 3 h of incubation, the fluorescence intensity of the DOX-loaded HMS@FTD nanocarriers (FA-conjugated) in the KB cells (folate receptor positive, Figure 5a, bottom panel) was

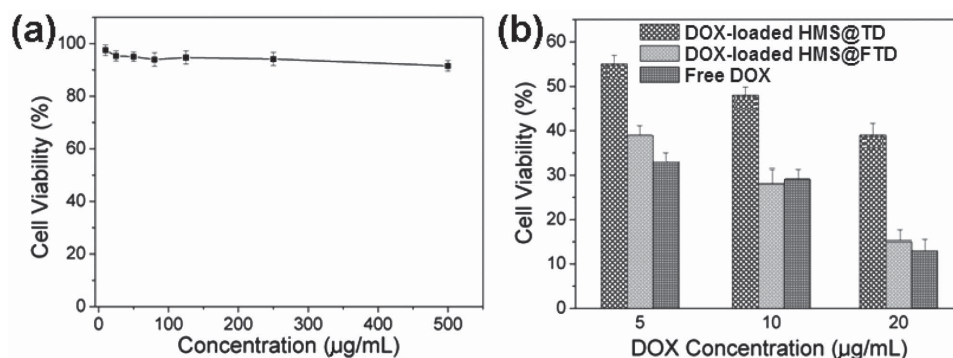


Figure 4. The viability of KB cells after incubation with a) DOX-free HMS@FTD nanocarriers, and b) DOX-loaded HMS@TD (left), DOX-loaded HMS@FTD nanocarriers (middle), and free DOX (right) for 24 h.

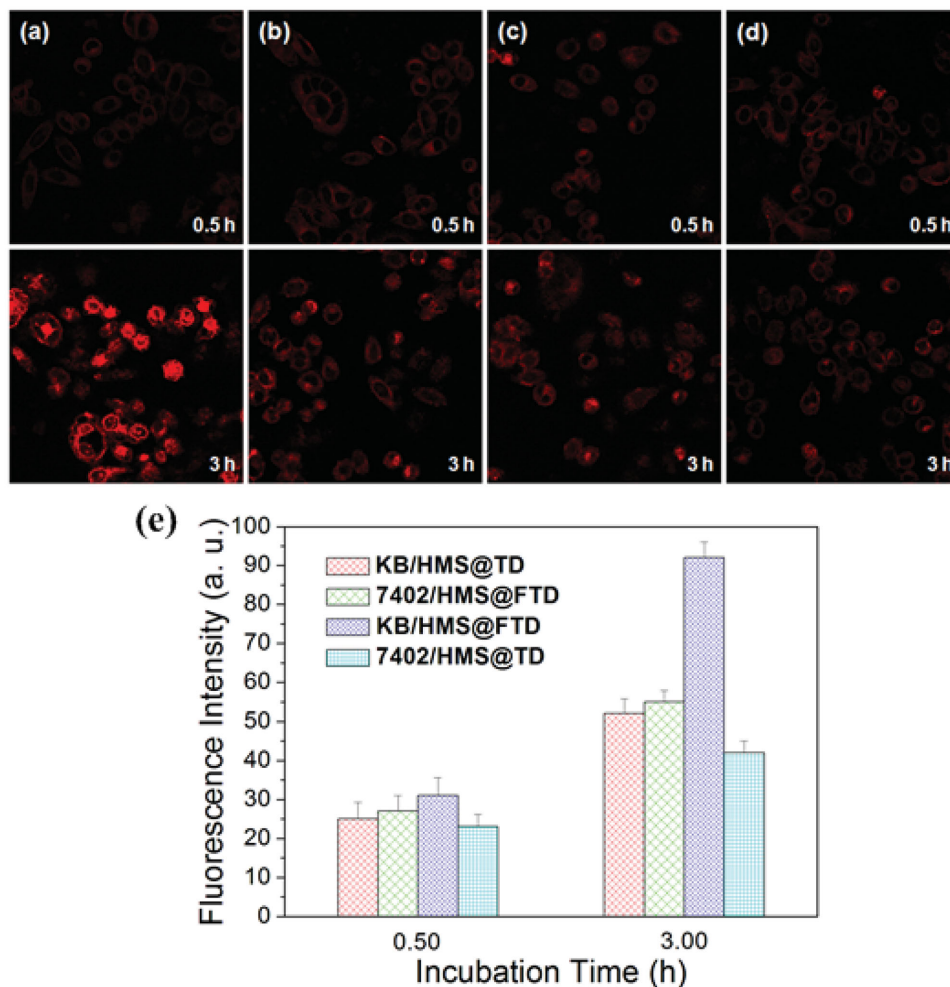


Figure 5. a,b) Representative CLSM images of incubation of DOX-loaded HMS@FTD nanocarriers in a) KB cells and b) 7402 cells for 0.5 h (top) and 3 h (bottom). c,d) CLSM images of incubation of DOX-loaded HMS@TD nanocarriers in c) KB cells and d) 7402 for 0.5 h (top) and 3 h (bottom). e) Mean fluorescence intensity (MFI) of DOX-loaded HMS@FTD nanocarriers in KB cells (blue) and 7402 cells (green); and DOX-loaded HMS@TD in KB cells (red) and 7402 cells (cyan) for 0.5 and 3 h.

significantly higher than that in the 7402 cells (folate receptor negative, Figure 5b, bottom panel). Similarly, after 3 h of incubation, the FA-conjugated nanocarriers (HMS@FTD, Figure 5a, bottom panel) in the KB cells also showed a much stronger intensity compared to that of the FA-free nanocarriers (HMS@TD, Figure 5c, bottom panel) in the same cancer cell line. These results further confirm that the direct internalization via folate-receptor-mediated endocytosis has greatly enhanced the uptake of the drug nanocarriers. Similar observations were observed in the flow cytometry studies, where the mean fluorescence intensity (MFI) was used to evaluate the uptake of the drug nanocarriers by the cells. As shown in Figure 5d, after 3 h of incubation, the FA-conjugated nanocarriers (HMS@FTD) showed a much higher MFI in the folate receptor positive cells (KB cells) than that in the other two systems [FA-conjugated nanocarriers (HMS@FTD) in the folate receptor negative cells (7402 cells) and FA-free nanocarriers (HMS@TD) in the folate receptor positive cells (KB cells)]. HeLa cells were also used in the flow cytometry studies, and the results are shown in Figure S4 (Supporting Information), which also confirm the targeting properties of

the FA-conjugated nanocarriers (HMS@FTD) in the folate receptor positive cells (KB and HeLa).

The *in vitro* studies showed that the DOX-loaded HMS@FTD nanocarriers were able to selectively deliver the drugs to the cancer cells with over-expressed folate receptors. To determine the maximum tolerance dose (MTD) of the DOX-loaded HMS@FTD nanocarriers, the nanocarriers were intravenously injected into healthy Balb/c mice at doses of 0 (used saline solution as the control), 20, 40, or 60 mg DOX per kg body weight. The mice showed morbidity if the highest dose of DOX (60 mg DOX per kg body weight) was intravenously administered. In contrast, the other mice groups, receiving lower doses of nanocarriers, were healthy and <10% weight loss was detected over two weeks. Therefore, the MTD of the HMS@FTD nanocarriers was around 40 mg DOX per kg body weight. This value is much higher (also an indicative of lower cytotoxicity) than that of free DOX (8 mg DOX per kg body weight). Figure S5 (Supporting Information) presents the *in vivo* pharmacokinetics of the HMS@FTD nanocarriers after their intravenous administration to mice. A slow decrease in the DOX concentration from the DOX-loaded

HMS@FTD nanocarriers was detected in the blood over 24 h after injection, which suggests that the HMS@FTD nanocarriers had a long systemic circulation and slow elimination in the blood. Such features are pivotal in designing efficient drug-delivery nanocarriers with a high clinical efficacy.

In vivo studies of the as-fabricated HMS@FTD nanocarriers were carried out using female athymic nude mice bearing HeLa (folate receptor positive) tumors with a tumor size of around 0.5 cm (after 3 weeks post inoculation of about 1×10^6 cells on the right foreleg) as the animal model. The fluorescence image (from the red-emitting RhB labeled on the HMS@FTD nanocarriers) was used to evaluate the uptake of the drug nanocarriers. As shown in **Figure 6b**, a strong fluorescence was observed in the tumor at around 24 h after the intravenous injection of the DOX-loaded HMS@FTD nanocarriers. In contrast, no visible fluorescence was detected in the tumor of the mice after 24 h if the fluorescent HMS NPs (without the FTD capping ligands) were injected intravenously (**Figure 6a**). This data provides supporting evidence for the crucial role of the multifunctional FTD capping ligands in the HMS@FTD nanocarriers. To further affirm the in vivo targeting capability of the FA ligands in

the HMS@FTD nanocarriers, a control experiment was carried out in which the mice were pre-dosed with excess folic acid (10 mg kg^{-1}) prior to the injection with the nanocarriers, which annulled almost all folate receptors in the tumor cells. As expected, after the intravenous injection of the HMS@FTD nanocarriers (24 h after injection), no obvious fluorescence (**Figure 6c**) was observed in the tumor site. This data further confirms the crucial role of the targeting FA ligands in the HMS@FTD nanocarriers.

To study the blood circulation of the nanocarriers, Blood was drawn at different time points post injection and solubilized by a lysis buffer. The HMS levels in the blood samples could be measured by UV-vis spectroscopy due to the modified FITC, according to previous reports. The blood circulation data of the HMS@FTD nanocarriers are shown in **Figure S6** in the Supporting Information, which confirms a long blood circulation half-life.

The in vivo distribution of the DOX-loaded HMS@FTD nanocarriers and the pristine fluorescent HMS NPs (without the amphiphilic FTD capping agents) is presented in **Figure 7**. The fluorescence intensity of the HMS@FTD nanocarriers in the tumor was significantly higher than that in other major organs. This intensity was also much stronger than that of the HMS NPs in the tumor, further demonstrating the high targeting efficiency of the designed FTD capping ligands. The HMS@FTD nanocarriers were also barely found in normal organs, indicating that the nanocarriers had a prolonged and sufficient blood circulation for the efficient targeting and delivery of the drugs to the tumor. The in vivo distribution of Si from the HMS@FTD nanocarriers was further examined by inductively coupled plasma atomic emission spectrometry (ICP-AES). As shown in **Figure S4** (Supporting Information), the results were also consistent with the biodistribution data from the fluorescence images (**Figure 7**, and **Figure S8**, Supporting Information), further confirming that the as-designed nanocarriers were mainly accumulated in the tumor. The suitable size of the as-designed nanocarrier in combination with its biocompatible PEG-like capping shell, may have led to its prolonged blood circulation, reduced nonspecific binding, and the final preferential deposition in the tumor. To further evaluate whether the improved biodistribution can enhance the anti-tumor efficacy, the changes in tumor size after intravenous injection of saline, pristine fluorescent HMS NPs, free DOX, and DOX-loaded HMS@FTD nanocarriers were investigated. As shown in **Figure 8**, the best tumor growth inhibition was a shrinkage to about 5.12% of the control group tumor, which was achieved in the

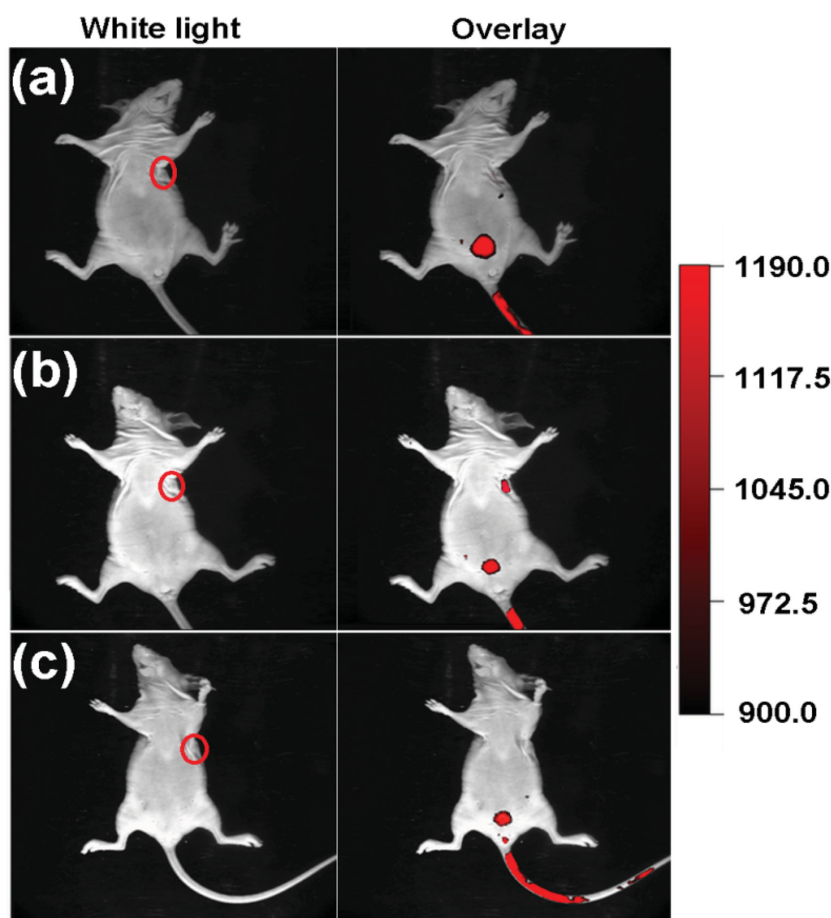


Figure 6. In vivo fluorescence images of the subcutaneous HeLa tumor-bearing athymic nude mice (right foreleg, indicated by the red circle) after an intravenous injection of 500 μL of a) fluorescent HMS NPs (1 mg mL^{-1}) and b) HMS@FTD nanocarriers (1 mg mL^{-1}). c) A blocking dose of folic acid was first injected into the mouse to neutralize the folate receptors in the tumor cells followed by an injection of 500 μL HMS@FTD nanocarriers (1 mg mL^{-1}). The fluorescence images were achieved at 24 h after injection.

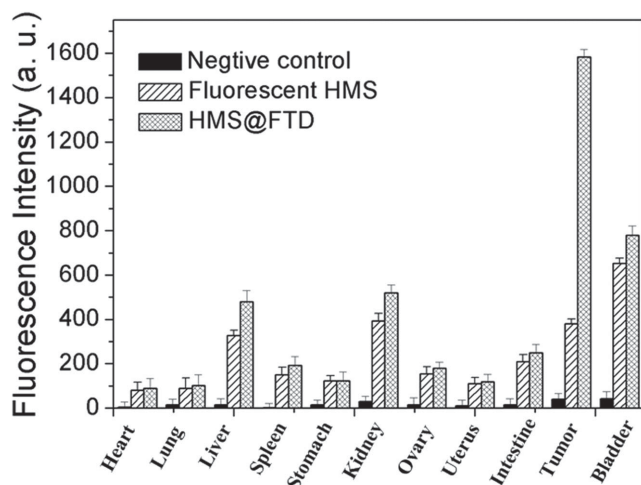


Figure 7. Fluorescence intensities of the dissected organs of sacrificed mice bearing the HeLa tumor 24 h after the intravenous injection of pristine fluorescent HMS NPs (green) or DOX-loaded HMS@FTD nanocarriers (blue).

mice group injected with DOX-loaded HMS@FTD nanocarriers. In contrast, no obvious inhibition was observed in the mice group injected with the pristine fluorescent HMS NPs. Free DOX showed an inhibitory effect to about 54.43% shrinkage of the tumor as compared to that of the control group. The amount of shrinkage is thus much lower than that of the DOX-loaded HMS@FTD nanocarriers. Taken together, these data confirmed that the incorporation of the FTD moieties in the as-designed drug carrier has significantly enhanced the antitumor efficacy on the systemic level.

3. Conclusions

A smart core-shell structured drug nanocarrier was developed in this study using HMS NPs as the core and specifically designed multifunctional amphiphilic FTD ligands as the encapsulating shell. The HMS NPs and amphiphilic FTD

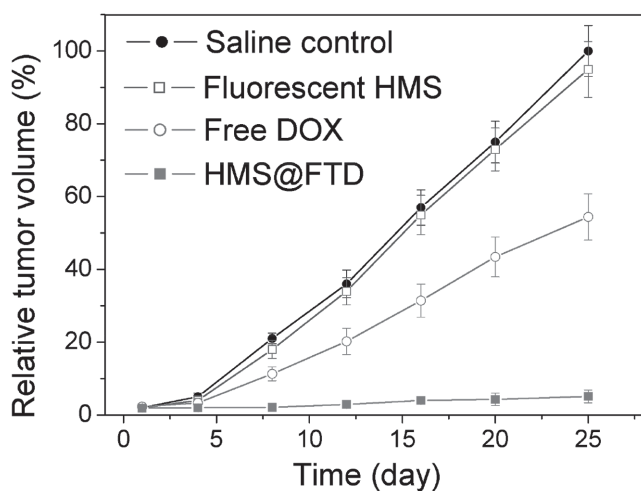


Figure 8. Changes in tumor volume after intravenous injection of saline, pristine fluorescent HMS NPs, free DOX, and DOX-loaded HMS@FTD nanocarriers in HeLa tumor-bearing nude mice.

ligands showed complementary properties (the HMS NPs provided a physical and structural stability and the FTP ligands provided the chemical specificity for tumor cell targeting). These properties were then independently tailored and integrated into a single HMS@FTD nanocarrier to achieve efficient and targeted drug delivery. Both in vitro and in vivo data suggested that the as-fabricated HMS@FTD nanocarriers are biocompatible and are able to deliver the hydrophobic drug to the target tumor cells. The nanocarriers could also unload the drug payload directly into the affected cells, where the weakly acidic environment inside the cells triggered the hydrolysis of the pH-labile linkages in the FTD capping ligands. The smart drug carrier in this study is a good prospect for further clinical studies.

4. Experimental Section

Chemicals: 1-bromododecane, *p*-toluenesulfonic acid (PTSA), anhydrous potassium carbonate, glycerol, di-*t*-butyl dicarbonate (BOC)-anhydride, folic acid, dicyclohexcarbodiimide (DCC) and *N*-hydroxysuccinimide (NHS) were purchased from Sinopharm Chemical Reagent Co. Ltd. (2-(Acryloyloxy)ethyl) trimethylammonium chloride (AETAC, 80 wt% in water), tetraethyl orthosilicate (TEOS), hexadecyltrimethylammonium bromide (CTAB, >99.0%), 2,2-azobis(2-methylpropionamide) dihydrochloride (V-50, >97.0%), fluorescein isothiocyanate (FITC), rhodamine B isothiocyanate (RhB), 3-aminopropyltriethoxysilane (APTES), 18-crown-6, octadecyltrimethoxysilane (OTMS), 4,7,10-trioxo-1,13-tridecanediamine (TDA), and cyanuric chloride were obtained from Sigma-Aldrich Co (Shanghai, China). Styrene (St, >99.0%) was washed through an inhibitor remover column and then distilled under reduced pressure prior to use. Other reagents were used as received. All of the animal procedures were performed in compliance with Soochow University Guidelines for the Care and Use of Laboratory Animals.

Synthesis of Hollow Mesoporous Silica (HMS) Nanoparticles: The templating polystyrene nanoparticles (PS NPs) were synthesized by an emulsifier-free emulsion polymerization. In a typical synthesis of 120 nm PS NPs, 500 mg of AETAC (80 wt% in H₂O) was dissolved in 180 g of water in a 500 mL round-bottomed flask, followed by a slow addition of 20 g of styrene. The mixed solution was stirred for 30 min, purged with nitrogen for 20 min, and heated up to 90 °C. A 5 mL aqueous solution containing 500 mg of V-50 was then introduced. The emulsion was kept at 90 °C for 24 h under nitrogen protection for the complete polymerization. The PS NPs were collected by centrifugation and washed copiously with ethanol for several times.

In a typical synthesis of the HMS NPs, 0.8 g of CTAB was first dissolved in a mixed solvent containing 80 g of water, 60 g of ethanol, and 1.5 mL of ammonium hydroxide solution (28%). 930 mg of PS NPs was then dispersed in water (10.0 g) by sonication. The dispersed PS NPs were added dropwise to the above CTAB solution at room temperature and under vigorous stirring. The mixed solution was sonicated for 10 min. The milky mixture was then stirred for 30 min followed by the addition of 4.0 g of TEOS. The mixture was kept stirring at room temperature for 12 h. The precipitate was washed copiously with ethanol and dried at room temperature. The product was then calcined in air at 600 °C for 6 h, which completely removed the templating PS NPs and the

pore-generating agents CTAB. The HMS NPs were then collected and stored in a desiccator.

Synthesis of Hydrophobic FITC or RhB-Doped Fluorescent HMS NPs: The preparation and modification of the organic dye (FITC or RhB) labeled HMS NPs were performed at room temperature. In brief, 190 mg of APTES was introduced into an ethanol solution (10 mL) containing 37 mg of FITC or RhB. The mixed solution was stirred for 10 h, and the resultant solution was added to 5 mL of ethanol solution containing 100 mg of HMS NPs. The reaction was allowed to proceed overnight, leading to the formation of fluorescent HMC NPs. To modify the surface of the fluorescent HMS NPs from hydrophilic to hydrophobic, 5 mL of OTMS was introduced into the HMS NP solution. The mixture was then stirred overnight. The product was collected by centrifugation, washed several times with acetonitrile and ethanol, and then dried under vacuum.

Synthesis of 4-n-dodecyloxybenzaldehyde (DBD): 1-bromododecane (29.9 g, 120 mmol) was added dropwise into the mixture of *p*-hydroxybenzaldehyde (12.2 g, 100 mmol) and anhydrous potassium carbonate (20.7 g, 150 mmol) in 150 mL of acetone. After heating under reflux with stirring for 14 h, the mixture was filtered off and acetone was removed by a rotary evaporator. The crude product was purified by column chromatography (ethyl acetate/petroleum ether, 1:10). Anal. Calcd. for $C_{19}H_{30}O_2$: C, 78.57%, H, 10.41%, O, 11.02%. Found: C, 78.48%, H, 10.53%, O, 10.99%. 1H NMR (400 MHz, $CDCl_3$), δ [ppm]: 9.88 (s, 1H), 7.83 (d, 2H), 6.99 (d, 2H), 4.04 (t, 2H), 1.86–1.76 (m, 2H), 1.46 (m, 2H), 1.26 (m, 16H, CH_2), 0.88 (t, 3H). ^{13}C NMR (75 MHz, $CDCl_3$) δ [ppm]: 191.12, 164.50, 132.24, 129.91, 114.96, 68.65, 32.16, 29.29–29.88, 26.19, 22.94, 14.39. High resolution mass spectrometer (HRMS) calcd. for $C_{19}H_{30}O_2$ [M+H]⁺ 291.2206, found 291.2211.

Synthesis of 4-n-dodecyloxybenzalacetal (DBA): In a typical synthesis, DBD (8.7 g, 30 mmol) was allowed to react with glycerol (2.76 g, 30 mmol) in 50 mL of toluene using PTSA (0.5 g) as a catalyst. The solution was refluxed under vigorous stirring for 14 h, and the water formed by the dehydrogenation reaction was removed by the oil/water separator. The mixture was then evaporated and washed with an aqueous solution of potassium carbonate (1 wt%, 80 mL) to remove the acid catalyst and the remaining glycerol. Afterwards, the precipitate was filtered off and purified by column chromatography (ethyl acetate-petroleum ether, 1:2). Anal. Calcd. for $C_{22}H_{36}O_4$: C, 72.49%, H, 9.95%, O, 17.56%. Found: C, 72.36%, H, 10.04%, O, 17.60%. 1H NMR (400 MHz, $CDCl_3$), δ [ppm]: 7.41 (d, 2H), 6.90 (d, 2H), 5.51 (s, 1H), 3.57–4.38 (m, 8H), 1.86–1.76 (m, 2H), 1.50–1.39 (m, 2H), 1.26 (m, 16H), 0.88 (t, 3H). ^{13}C NMR (75 MHz, $CDCl_3$), δ [ppm]: 191.15, 132.25, 127.36, 114.48, 101.93, 72.48, 68.28, 64.21, 32.17, 29.29–29.88, 26.22, 22.95, 14.39. HRMS calcd. for $C_{22}H_{36}O_4$ [M+H]⁺ 365.5126, found 365.5121.

Synthesis of BOC-4,7,10-trioxa-1-tridecanamine (BOC-TDA): 3.7 g of TDA was dissolved in 1,4-dioxane (80 mL) and treated with BOC-anhydride (1.8 g). The mixture was stirred at room temperature overnight, followed by the removal of the solvent. The resulting yellow oil was purified by silica gel chromatography (methanol-dichloromethane, 1:10). 1H NMR (400 MHz, $CDCl_3$), δ [ppm]: 5.00 (s, 1H), 3.52–3.48 (m, 12H), 3.20 (d, 2H), 2.79 (t, 2H), 1.71–1.65 (m, 4H), 1.58 (s, 2H), 1.42 (s, 9H). ^{13}C NMR (75 MHz, $CDCl_3$), δ [ppm]: 155.6, 69.5–68.9, 66.2, 48.5, 36.9, 30.2, 28.5, 27.2.

Synthesis of FA-4,7,10-trioxa-1-tridecanamine (FA-TDA): 0.62 g of DCC and 0.51 g of NHS were mixed with 50 mL of dry dimethylformamide solution containing 2.0 g of folic acid. The mixed solution

was stirred for 12 h at room temperature in the dark. The solution was then filtered off and precipitated in diethyl ether. The resulting yellow powder was washed several times with anhydrous ether and used immediately for the next step. FA-NHS (1.2 g, 2.2 mmol) was completely dissolved in 100 mL of dry pyridine, followed by a slow addition of BOC-TDA (0.73 g, 2.27 mmol) over 30 min. The mixture was stirred for 12 h at room temperature in the dark. After evaporating the pyridine, the resulting compound was dissolved in 5 mL of trifluoroacetic acid (TFA) to remove the BOC group. The deprotection step was carried out at room temperature for 4 h. TFA was then removed under vacuum. The resulting compound was loaded on a DEAE Sephadex A25 column packed with potassium tetraborate, and the compound was eluted with 10–50 mM ammonium bicarbonate. All fractions were collected and lyophilized. 1H NMR (400 MHz, $DMSO-d_6$), δ [ppm]: 8.60 (s, 1H), 8.08–7.76 (m, 6H), 6.75 (d, 2H), 4.56 (s, 2H), 4.40–4.76 (m, 1H), 3.68–3.37 (m, 14H), 3.37 (d, 2H), 2.88–2.82 (m, 2H), 2.53 (s, 2H), 2.39–2.21 (m, 2H), 1.76 (t, 2H), 1.60–0.92 (m, 4H). ^{13}C NMR (75 MHz, $DMSO-d_6$), δ [ppm]: 175.0, 172.9, 166.9, 161.3, 158.5, 153.6, 151.8, 148.7, 130.0, 128.8, 121.8, 111.9, 70.3–69.3, 68.8, 67.5, 46.2, 36.9, 35.7, 30.2, 29.3, 27.2.

Synthesis of 2,4-dichloro-dodecyloxybenzalacetal-1,3,5-triazine (TsT-DBA) and FA-TDA-DBA: 423 mg of potassium carbonate and 25 mg of 18-crown-6 were added to 10 mL of a toluene solution containing 568 mg of cyanuric chloride. DBA (1.1 g) in 5 mL of toluene was then added dropwise under nitrogen. The reaction was allowed to proceed under refluxing for around 18 h. The product was collected, passed through a plug of Celite, concentrated in a rotary evaporator, and dried overnight under vacuum. The FA-TDA was conjugated following the procedures described above to obtain FA-TDA-DBA. 1H NMR (400 MHz, $DMSO-d_6$), δ [ppm]: 8.60 (s, 1H), 7.82–6.95 (m, 10H), 6.65 (d, 2H), 5.21 (s, 2H), 4.40–3.58 (m, 10H), 3.48–2.90 (m, 16H), 2.88 (d, 2H), 2.49–2.36 (m, 2H), 1.73 (d, 2H), 1.70–1.41 (m, 4H), 1.61–0.90 (m, 24H). Anal. Calcd. for $C_{54}H_{75}ClN_{12}O_{12}$: C, 57.92%, H, 6.75%, Cl, 3.17%, N, 15.01%, O, 17.15%.

Loading and Release Profiles of Drugs in the As-fabricated HMS@FTD Nanocarriers: Doxorubicin (DOX) was chosen as the model drug to evaluate the loading and release profiles in the as-fabricated HMS@FTD nanocarriers. The water-insoluble DOX was extracted from doxorubicin hydrochloride (DOX-HCl).^[48] The DOX solution (5 mg mL⁻¹) was added to 0.8 mL of the as-prepared HMS and FA-TDA-DBA in tetrahydrofuran, followed by a slow addition of 10 mL of phosphate buffer (0.02 M, pH 7.4). The mixed solution was shaken for 24 h to allow the diffusion of DOX into the NPs. The DOX-loaded HMS@FTD nanocarriers were then centrifuged, and the free DOX was removed. The concentration of free DOX in solution was determined by measuring the UV absorbance at 485 nm. To determine the amount of drugs encapsulated inside the nanocarriers, a standard plot was prepared under identical conditions.

The free DOX concentration was studied after the centrifugation and the loading efficiency was calculated as follows:

$$\text{loading efficiency} = (C_0V_0 - C_tV_t)/C_0V_0 \quad (1)$$

where C_0 and V_0 were the concentration and volume of the added DOX, and C_t , V_t were the concentration and volume of the free DOX after centrifugation. To assure the accurate determination of this value, the experiments were carried out three times and a mean value was achieved.

The drug-release test was performed by suspending the DOX-loaded HMS@FTD nanocarriers in phosphate-buffered saline (PBS) buffer (pH 7.4). The mixed solution was shaken in a water bath at a constant temperature of 37 °C. To determine the release amount of the drug at a particular time, 1.0 mL of the solution was withdrawn after centrifugation, and the same volume of PBS buffer was introduced to keep a constant volume. To determine the release amount at a particular pH, the obtained colloid was adjusted to a certain pH by acetate buffer. The drug concentration in the withdrawn solution was analyzed by measuring the UV absorbance at 485 nm. The experiments were conducted in triplicate and the results were presented as an average value with standard deviations.

Cell Culture and Preparation: Human epidermoid carcinoma (KB cells, with over-expressed folate receptors or FR positive) and hepatoma 7402 (without over-expressed folate receptors or FR negative) cell lines (purchased from Shanghai Cell Institute Country Cell Bank, P. R. China) were cultured at 37 °C in a humidified incubator (5% CO₂ in air, v/v) as a monolayer in the RPMI-1640 medium supplemented with 10% of heat-inactivated fetal bovine serum.

In Vitro Cytotoxicity: Sulforhodamine B (SRB) assay was used to assess the potential cytotoxicity of the as-fabricated drug carriers. In brief, hepatoma 7402 or KB cells were seeded in 96-well plates (1.3 × 10⁴ cells per well). Four duplicate wells were set up for each sample. The culture medium was replaced with the medium containing different concentrations of DOX-free or DOX-loaded HMS@FTD nanocarriers, and then cultured at 37 °C in a humidified incubator (5% CO₂ in air, v/v). After 72 h, the medium was poured away and 10% (w/v) trichloroacetic acid in Hank's balanced salt solution (100 μL) was added, and stored at 4 °C for 1 h. The stationary liquid was then discarded, and the cells were washed with copious amounts of water for five times before air drying and they were then stained with 0.4% (w/v) SRB solution (100 μL per well) for 30 min at room temperature. After the removal of free SRB, the cells were washed with 0.1% acetic acid solution for five times. The bound SRB dye was solubilized in a 10 mmol L⁻¹ tris-base buffer (150 μL, pH 10.5). The optical density (OD) was determined by the optical absorbance at 531 nm of individual wells by a spectrophotometer.

Cellular Uptake of DOX-Loaded HMS@FTD Nanocarriers: The KB cells and Hepatoma 7402 cells were seeded in 96-well plates (1.3 × 10⁴ cells per well) and incubated overnight at 37 °C in a humidified incubator. The dispersion was prepared in RPMI-1640 medium. The DOX concentration in the HMS@FTD (FA-conjugated) and HMS@TD (FA-free) nanocarriers was identical, namely 10 μg mL⁻¹. The cells were washed twice with PBS buffer and incubated with the above solutions for 0.5 or 3 h. The culture media were removed and the cells were washed three times with PBS buffer before testing. The cells were observed under a Nikon AY laser scanning confocal microscope. All images were gathered at the same settings and processed with Nikon AY software.

Flow Cytometry Study of the Uptake of DOX-loaded HMS@FTD Nanocarriers: Hepatoma 7402 and KB cells were cultured as a monolayer in RPMI-1640 medium supplemented with 10% heat-inactivated fetal bovine serum. The medium was then replaced with freshly prepared medium containing DOX-loaded HMS@FTD or HMS@TD nanocarriers with an equivalent DOX concentration of 10 μg mL⁻¹. The cells were incubated for 3 h. The suspensions

were then centrifuged, washed three times with cold PBS buffer, and resuspended in PBS buffer. Flow cytometry was performed on a BD FACS Calibur instrument.

Tumor Xenografts and In Vivo Imaging: HeLa tumor cells were harvested by centrifuging, and resuspending in sterile PBS buffer. The tumor cells (1 × 10⁶ cells/site) were then implanted subcutaneously into the right foreleg of female athymic nude mice (4 weeks old). Biodistribution and imaging studies were performed when the tumor size reached around 0.5 cm (3 weeks after post-inoculation). In vivo fluorescence imaging was performed on a Kodak DXS 4000 PRO system. The fluorescence intensities were analyzed using Kodak Molecular Imaging Software.

Supporting Information

Supporting Information is available from the Wiley Online Library or from the author.

Acknowledgements

This work was supported by the Collaborative Innovation Center of Suzhou Nano Science and Technology. The authors gratefully acknowledge the financial support provided by the National Natural Science Foundation of China (21336005, 21301125), the Natural Science Foundation of Jiangsu Province (BK2012625), and the Suzhou Nano-project (ZXG2013001, ZXG201420).

- [1] S. H. Medina, M. E. H. El-Sayed, *Chem. Rev.* **2009**, *109*, 3141.
- [2] C. M. Cobley, J. Chen, E. C. Cho, L. V. Wang, Y. Xia, *Chem. Soc. Rev.* **2011**, *40*, 44.
- [3] R. Hao, R. Xing, Z. Xu, Y. Hou, S. Gao, S. Sun, *Adv. Mater.* **2010**, *22*, 2729.
- [4] C. Minelli, S. B. Lowe, M. M. Stevens, *Small* **2010**, *21*, 2336.
- [5] K. Y. Win, E. Ye, C. P. Teng, S. Jiang, M. Y. Han, *Adv. Healthcare Mater.* **2013**, *2*, 1571.
- [6] R. H. Xiong, S. J. Soenen, K. Braeckmans, A. G. Skirtach, *Theranostics* **2013**, *3*, 141.
- [7] W. J. M. Mulder, G. J. Strijkers, G. A. F. van Tilborg, D. P. Cormode, Z. A. Fayad, K. Nicolay, *Acc. Chem. Res.* **2009**, *42*, 904.
- [8] J. L. Vivero-Escoto, I. I. Slowing, B. G. Trewyn, V. S. Y. Lin, *Small* **2010**, *6*, 1952.
- [9] J. Gao, H. Gu, B. Xu, *Acc. Chem. Res.* **2009**, *42*, 1097.
- [10] A. Z. Wang, V. Bagalkot, C. C. Vasiliou, F. Gu, F. Alexis, L. Zhang, M. Shaikh, K. Yuet, M. J. Cima, R. Langer, P. W. Kantoff, N. H. Bander, S. Jon, O. C. Farokhzad, *ChemMedChem* **2008**, *3*, 1311.
- [11] A. G. Skirtach, C. Dejugnat, D. Braun, A. S. Susha, A. L. Rogach, W. J. Parak, H. Möhwald, G. B. Sukhorukov, *Nano Lett.* **2005**, *5*, 1371.
- [12] X. Mei, D. Chen, N. Li, Q. Xu, J. Ge, H. Li, J. Lu, *Microporous Mesoporous Mater.* **2012**, *152*, 16.
- [13] Y. Chen, H. R. Chen, D. P. Zeng, Y. B. Tian, F. Chen, J. W. Feng, J. L. Shi, *ACS Nano* **2010**, *4*, 6001.
- [14] T. Liu, L. Li, X. Teng, X. Huang, H. Liu, D. Chen, J. Ren, J. He, F. Tang, *Biomaterials* **2011**, *32*, 1657.
- [15] T. Wang, F. Chai, Q. Fu, L. Zhang, H. Liu, L. Li, Y. Liao, Z. Su, C. Wang, B. Duan, D. Ren, *J. Mater. Chem.* **2011**, *21*, 5299.

- [16] X. Jiang, T. L. Ward, Y. S. Cheng, J. Liu, C. J. Brinker, *Chem. Commun.* **2010**, 46, 3019.
- [17] Y. Zhu, Y. Fang, L. Borchardt, S. Kaskel, *Microporous Mesoporous Mater.* **2011**, 141, 199.
- [18] Y. F. Zhu, J. L. Shi, W. H. Shen, X. P. Dong, J. W. Feng, M. L. Ruan, Y. S. Li, *Angew. Chem., Int. Ed.* **2005**, 44, 5083.
- [19] Y. Zhao, L. N. Lin, Y. Lu, S. F. Chen, L. Dong, S. H. Yu, *Adv. Mater.* **2010**, 22, 5255.
- [20] A. K. Bajpai, S. K. Shukla, S. Bhanu, S. Kankane, *Prog. Polym. Sci.* **2008**, 33, 1088.
- [21] S. Ganta, H. Devalapally, A. Shahiwala, M. Amiji, *J. Controlled Release* **2008**, 126, 187.
- [22] W. Xiao, W. H. Chen, X. D. Xu, C. Li, J. Zhang, R. X. Zhuo, *Adv. Mater.* **2011**, 23, 3526.
- [23] L. Linderth, G. H. Peters, R. Madsen, T. L. Andresen, *Angew. Chem., Int. Ed.* **2009**, 48, 1823.
- [24] A. Laromaine, L. Koh, M. Murugesan, R. V. Ulijn, M. M. Stevens, *J. Am. Chem. Soc.* **2007**, 129, 4156.
- [25] H. Cheng, P. S. Hill, D. J. Siegwart, N. Vacanti, A. K. R. Lytton-Jean, S. W. Cho, A. Ye, R. Langer, D. G. Anderson, *Adv. Mater.* **2011**, 23, H95.
- [26] M. Delcea, H. Möhwald, A. Skirtach, *Adv. Drug Delivery Rev.* **2011**, 63, 730.
- [27] M. A. Cohen Stuart, W. T. S. Huck, J. Genzer, M. Müller, C. Ober, M. Stamm, G. B. Sukhorukov, I. Szleifer, V. V. Tsukruk, M. Urban, F. Winnik, S. Zauscher, I. Luzinov, S. Minko, *Nat. Mater.* **2010**, 9, 101.
- [28] J. Luten, C. F. V. Nostrum, S. C. D. Smedt, W. E. Hennink, *J. Controlled Release* **2008**, 126, 97.
- [29] D. Chen, N. Li, H. Gu, X. Xia, Q. Xu, J. Ge, J. Lu, Y. Li, *Chem. Commun.* **2010**, 46, 6708.
- [30] C. Ding, J. Gu, X. Qu, Z. Yang, *Bioconjugate Chem.* **2009**, 20, 1163.
- [31] V. P. Torchilin, *Adv. Drug Delivery Rev.* **2006**, 58, 1532.
- [32] M. Guo, C. Que, C. Wang, X. Liu, H. Yan, K. Liu, *Biomaterials* **2011**, 32, 185.
- [33] N. Nasongkla, E. Bey, J. Ren, H. Ai, C. Khemtong, J. S. Guthi, S. F. Chin, A. D. Sherry, D. A. Boothman, J. Gao, *Nano Lett.* **2006**, 6, 2427.
- [34] H. Kawaguchi, *Prog. Polym. Sci.* **2000**, 25, 1171.
- [35] L. Wang, K. G. Neoh, E. T. Kang, B. Shuter, *Biomaterials* **2011**, 32, 2166.
- [36] Y. Gao, Y. Chen, X. Ji, X. He, Q. Yin, Z. Zhang, J. Shi, Y. Li, *ACS Nano* **2011**, 5, 9788.
- [37] A. Verma, F. Stellacci, *Small* **2010**, 6, 12.
- [38] M. S. Shim, C. S. Kim, Y. C. Ahn, Z. Chen, Y. J. Kwon, *J. Am. Chem. Soc.* **2010**, 132, 8316.
- [39] T. Zhang, Z. Cheng, Y. Wang, Z. Li, C. Wang, Y. Li, Y. Fang, *Nano Lett.* **2010**, 10, 4738.
- [40] C. E. McNamee, M. Kappl, H. J. Butt, K. Higashitani, K. Graf, *Langmuir* **2010**, 26, 14574.
- [41] L. Z. Zhao, J. J. Peng, Q. Huang, C. Y. Li, M. Chen, Y. Sun, Q. N. Lin, L. Y. Zhu, F. Y. Li, *Adv. Funct. Mater.* **2014**, 24, 363.
- [42] Y. Chen, Q. S. Meng, M. Y. Wu, S. G. Wang, P. F. Xu, H. R. Chen, Y. P. Li, L. X. Zhang, L. Z. Wang, J. L. Shi, *J. Am. Chem. Soc.* **2014**, 136, 16326.
- [43] Y. Yang, J. S. Jiang, B. Du, Z. F. Gan, M. Qian, P. Zhang, *J. Mater. Sci.: Mater. Med.* **2009**, 20, 301.
- [44] W. R. Zhao, M. D. Lang, Y. S. Li, L. Lia, J. L. Shi, *J. Mater. Chem.* **2009**, 19, 2778.
- [45] J. Sudimack, R. J. Lee, *Adv. Drug Delivery Rev.* **2000**, 41, 147.
- [46] H. Yuan, K. Luo, Y. Lai, Y. Pu, B. He, G. Wang, Y. Wu, Z. Gu, *Mol. Pharmaceutics* **2010**, 7, 953.
- [47] T. K. Jain, M. A. Morales, S. K. Sahoo, D. L. Leslie, *Mol. Pharmaceutics* **2005**, 2, 194.
- [48] C. Yan, J. K. Kepa, D. Siegel, I. J. Stratford, D. Ross, *Mol. Pharmacol.* **2008**, 74, 1657.

Received: October 15, 2015
Published online: November 30, 2015